Stiffness Characterization and Micromanipulation for Biomedical Applications using the Vision-based Force-Sensing Magnetic Mobile Microrobot

Georges Adam¹, Mazin Hakim², Luis Solorio², and David J. Cappelleri¹

Abstract—This paper presents the use of a micro-force sensing mobile microrobot (\$\mu FSMM\$) for in vitro biomedical applications. The \$\mu FSMM\$ utilizes a vision-based force sensor end-effector, which computes the force based on the deflection of a compliant structure with a known stiffness using a computer vision tracking algorithm. The \$\mu FSMM\$ is used to characterize the stiffness of several different alginate and hyaluronic acid hydrogel spheroid samples, which are typically used in 3D tissue engineered constructs for studying cellular behavior. Additionally, \$\mu FSMM\$ is used to perform safe micromanipulation tasks with these spheroids. These experimental results showcase some of the applications of this unique microrobot design in the fields of mechanobiology, theranostics, and force-guided micromanipulation.

I. INTRODUCTION

Nano- and microscale robotics show great promise in numerous fields of engineering and science, with a wide range of applications and great design flexibility. The major challenges associated with these types of robots are usually encountered during the fabrication, actuation, and control. While there are multiple actuation methods commonly used for microrobotic applications, such as [1], [2], [3], [4], this work showcases a magnetic field driven mobile microrobot. This external actuation method allows for different motion control methods [5], [6] and even closed-loop control [7] when pairing with a vision system for feedback.

In order to realize their full potential, it is essential for microrobots to possess sensing capabilities, allowing them to intelligently interact with the surrounding environment. Force sensing capabilities, for example, would enable the microrobot to report important material properties of its environment such as modulus, viscosity, and stiffness. For biological contexts, the implications of microscale mechanical characterization of materials is vast. The accurate mechanical characterization of biological materials (tissue, cells, and engineered hydrogels) is crucial to understanding cell behavior and is of high importance in tissue engineering. Mechanobiology [8], [9] studies how physical forces contribute to cell development, differentiation, and disease. The field revealed the importance of the process of mechanotransduction [10], hinting to the importance of safe cell

This work was supported by NSF Award NRI 1637961 and NIH Award R00CA198929. (Corresponding author: David J. Cappelleri.)

²Weldon School of Biomedical Engineering, Purdue University, West Lafayette, IN 47907, USA. {mhakim, lsolorio}@purdue.edu

manipulation and accurate force application, especially when single cell micromanipulation comes into play. Additionally, the ability to do this at the microscale with delicate biological samples saves materials, money and increases throughput when compared to traditional macroscale instruments. In this context, real-time micro-force sensing mobile microrobots can play a crucial role.

Furthermore, mobile microrobots can play a huge role in cell manipulation and arrangement, especially in tissue engineering applications in which precise arrangements of cells and other biological materials are of great importance. The addition of the micro-force sensing mechanism increases the breath of possible applications, making biomanipulation more reliable and safer, since it allows the implementation of control algorithms based on the visual tracking system. These applications include fundamental mechanobiology studies, intelligent biomanipulation tasks, and advanced theranostic applications [11], [12].

In general, micro-force sensing has been achieved using numerous techniques, which include capacitive MEMS devices [13], [14], atomic force microscope (AFM) probes [15], [16], piezoelectric [17], [18] and piezoresistive [19] techniques, among others. Most of these methods rely on fixed probes or sensors, which makes them difficult to integrate into standard biological test-beds, such as an inverted microscope. Additionally, these types of sensors usually don't have the necessary force sensing range, or are too expensive, requiring complex electronics, making it difficult to be used as a multipurpose micromanipulation and sensing tool. A vision-based force sensor [20], [21] provides a great solution to these problems, since it can be easily integrated on a mobile microrobot, providing accurate μ N-level resolution while being extremely inexpensive and simple to implement.

In previous works [22], [23], we have presented the micro-force sensing mobile microrobot (μ FSMM) that can perform on-board real-time micro-force sensing by optically measuring the displacement of a calibrated compliant structure. Using colored fiducials, a color tracking algorithm is employed to track the deformation of a soft polydimethyl-siloxane (PDMS) spring structure in real-time, resulting in real-time force feedback to the user. The microrobot has a magnetic nickel body, which allows it to be controlled using gradient magnetic fields. In this paper, we show some of the *in vitro* biomedical applications of this powerful tool, including stiffness measurements of different materials used in tissue engineering and other bioapplications, as well as

¹Multi-Scale Robotics and Automation Lab, School of Mechanical Engineering, Purdue University, West Lafayette, IN 47907, USA. {adamg, dcappell}@purdue.edu

safe micromanipulation of these biological testing materials.

II. MICROROBOT DESIGN OVERVIEW

An image of the μ FSMM along with some different endeffector designs is shown in Fig. 1. The microrobot consists of a hard silicon body, a PDMS compliant structure used for the vision-based micro force sensor, colored fiducials used to aid the tracking algorithm, and a nickel piece (not pictured) to make the μ FSMM responsive to external magnetic fields. For the different body designs explored, the microrobot footprint slightly changes, but the geometry of the compliant structure remains the same. The $\mu FSMM$ is a very flexible tool, since it can be specifically tailored depending on application. The end-effectors shown in Fig. 1 can each be used for targeted applications, making the micromanipulation or mechanical characterization process more effective. Furthermore, the stiffness of the PDMS compliant structure can also be tuned. This is done by adjusting the mixing ratio between the monomer and the cross linking agent in the fabrication procedure. A higher ratio will effectively reduce the stiffness of the structure, allowing it to measure forces in the low- μ N range.

In order to actuate the microrobots, a two dimensional gradient magnetic field is generated using the custom electromagnetic coils system shown in Fig. 2. The coil system frame was 3D printed and designed to fit under an inverted microscope, a typical component of biomedical research test-beds. This way, it is easy to work in different environments and use the μ FSMM in a wide range of applications. The vision-system consists of a 1.3 MP CMOS Camera (PointGrey e2v EV76C560), with an adjustable zooming lens that ranges from 0.75x to 4.5x. The system illumination is achieved with an LED ring placed underneath the coil system. A 3D mouse (3D Connexion) is used for the teleoperated position and orientation control of the microrobot.

Alternate End-Effectors PDMS Compliant Structure PDMS Colored Fiducials 1283µm 735µm

Fig. 1. The μ FSMM: The microrobot consists of a rigid silicon body and end-effector, compliant PDMS spring, and PDMS colored markers. The dimensions shown for the overall width and height of the robot vary from 719 μ m to 735 μ m and 1144 μ m to 1283 μ m, respectively. The thickness of the microrobot and compliant structure is approximately 80 μ m.

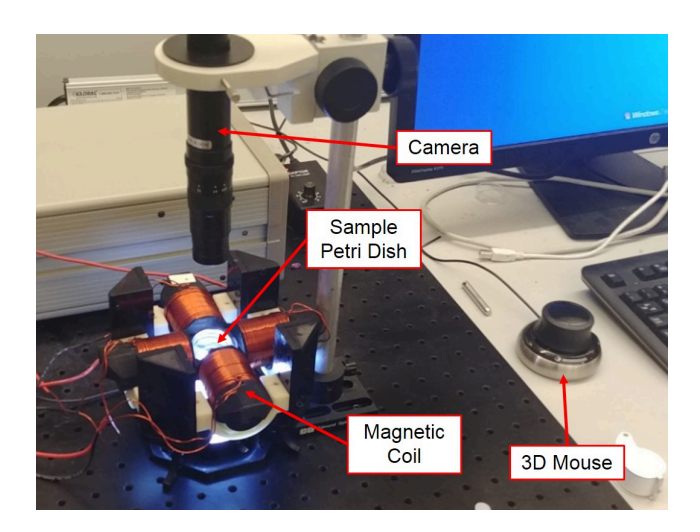


Fig. 2. Experimental setup used to control the μ FSMM. It consists of a pair of perpendicular electromagnetic coils, a camera system, and 3D mouse.

The microfabrication process of the μ FSMM consists of several photolithography steps followed by a deep reactive ion etching (DRIE) process. Each of the PDMS structures are patterned individually, with and the etching process creating trenches where the PDMS is deposited. Once the PDMS layers are cured, the microrobot body is patterned and etched, followed by a backside etching of windows to remove the completed microrobots. Since a silicon-only body will not respond to magnetic fields, a nickel (Ni) magnetic piece (approximately $250\mu m \times 500\mu m$) is fabricated separately using a chemical etching process (www.fotofab.com) and then assembled manually to the body of the microrobot using tweezers and glue. More details on the specific fabrication steps can be found in [22].

III. VISION-BASED MICRO-FORCE SENSING

A vision-based force sensor uses the principles of Hooke's law to measure force from observing the displacement of a material or structure of known stiffness. According to it, the force can be computed by multiplying the stiffness by the deflection. Therefore, there are two main components to the vision-based micro-force sensor: 1.) the stiffness calibration of the PDMS compliant structure in the X and Y directions; and 2.) the image-processing algorithm used to track the displacement of the compliant body. Each of these components are described in detail in the following sections.

A. Stiffness Calibration

In order to provide accurate force measurements, each microrobot has the stiffness of its compliant structure calibrated. The calibration is conducted in both the X and Y directions (K_x and K_y , respectively), as shown in Fig. 3 (a)-(b). This is done using a MEMS micro-force sensor (FT-S100, FemtoTools) mounted on a micromanipulator system (MP-225, Sutter Instruments) that is able to independently translate in three orthogonal directions with a resolution of 1 μ m per step size or smaller. The forces measured by the MEMS force sensor are recorded for several end-effector deflections, set by the micromanipulator position. This data is then plotted, as shown in Fig. 3(c), and the

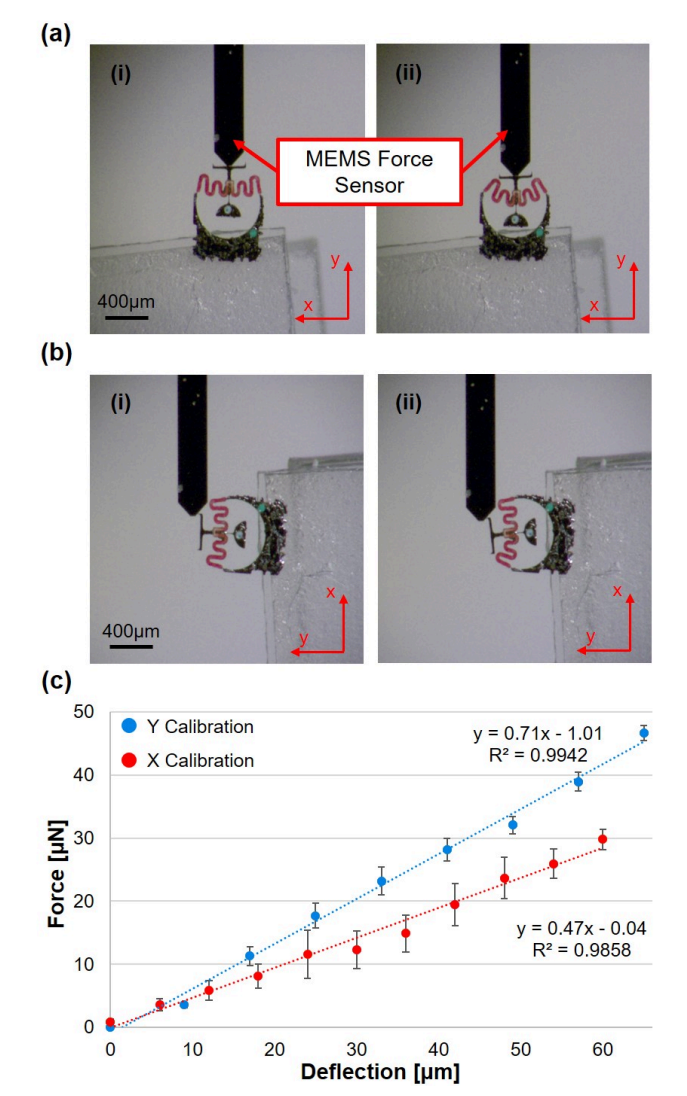


Fig. 3. μ FSMM compliant structure stiffness calibration process: (a) Calibration with MEMS micro force sensor in the Y direction and (b) in the X direction. Here, (i) represents the initial position (undeflected), and (ii) represents the final position. (c) Resultant calibration plot with stiffness in both directions. For this μ FSMM, K_x =0.47 N/m and K_y =0.71 N/m.

stiffness in both directions analyzed by calculating the slope of each linear fit. There are several factors that affect the final stiffness of the compliant structure. Most prominently, the PDMS mixing ratios have great effect on the overall stiffness. Additionally, the amount of colored dye present also changes the stiffness. All of these values can have slight variations, even on robots fabricated on the same silicon wafer. Therefore, it is crucial that every μ FSMM is calibrated individually to ensure accurate force measurements.

B. Image Processing Algorithm

In order to sense micro-forces using the μ FSMM, the displacement between the end-effector and the body of the microrobot needs to be determined accurately. To do that, a color tracking computer vision algorithm is used. The tracking algorithm employed is based on two color masks, which define areas of interest to be tracked for the colored fiducials on the body and end-effector of the microrobot. At first, the HSV (hue, saturation, and value) parameters are set

for each different fiducial (red, green, or blue), thus creating a thresholding mask for each marker. Using these masks, the position of the fiducials are known, and by tracking the relative magnitude and orientation of the vector connecting the two, the μ FSMM pose and compliant structure deflection are measured. The measured value is then converted to μ m using the conversion ratio from pixels to distance, which depends on the zoom level (typically around 6 μ m/pixel). Lastly, as an additional feature to make the algorithm run slightly faster, the user can select a region of interest (ROI) around the microrobot during the initialization of the code, which reduces the area that the thresholding mask is applied. The ROI remains the same size throughout the process, however its position moves along with the microrobot.

IV. BIOMEDICAL EXPERIMENTS

As cells push and pull on the surrounding extracellular matrix (ECM), they act, in a sense, the same as the force sensing microrobots described. Manipulating and interacting with their environment, cells can relay information about stiffness and rigidity of the ECM to their nucleus, however via complex biochemical machinery, they are then able to use this information to induce changes in transcription, differentiation [24], motility [25], and even progression of pathological conditions [26]. As Dupont and coworkers demonstrate, the activity and localization of transcriptional regulators YAP and TAZ are determined by ECM elasticity and the forces acting on the cytoskeleton, allowing different messages to be sent to the nucleus for coordinating cellular actions in mechanically different environments [27]. Consequently, the ability to characterize stiffness of in vitro tissue engineered 3D cultures, such as microscale ECM spheroids, can affords researchers more data on cellular behavior. Creative techniques to measure microscale cell spheroids and tissues include microfluidic devices [28], [29], cavitation rheology [30], and microtweezers [31]. In all of these methods, the tissue engineered constructs are subject to potentially high shear rates that may mechanically induce undesired transcriptional changes in experiments studying cells. Here, we are pioneering the use of μ FSMM to analyze the stiffness of such microscale ECM spheroids constructs.

As stated earlier, the cell is a complex feedback system that can both detect changes in extracellular forces and respond with various biochemical, pathological, migrational, functions. In biomanipulation experiments where sample preservation is key, it is important that the forces are limited in magnitude and time scale such that they do not interfere with any cellular function. Therefore, we have used the force sensing capabilities of the μ FSMM for a series of these biomanipulation experiments with the microscale ECM spheroids. This ensures their safe manipulation for eventual tissue engineering experiments and as analogs for manipulating living cells.

Two types of microscale acellular ECM spheroids were fabricated for stiffness characterization and biomanipulation tests. They were hydrogel capsules with different concentrations of alginate and hydrogel capsules with different concentrations of hyaluronic acid. To fabricate these spheroid constructs, the hydrogel solutions were printed using a BIO X 3D bioprinter (Cellink, Sweden) with an Elecromagnetic Droplet print-head. Sodium alginate (MP Biomedicals, 218295) was prepared in calcium and magnesium free phosphate buffered saline (PBS), pH 7.4 (Gibco, 70011-044) at 0.5% and 1% (w/v). Sodium hyaluronate (Lifecore Biomedical, HA15M-1) was methacrylated to allow photocrosslinking during fabrication and was prepared at concentrations of 2% and 4% (w/v) [32].

Solutions were loaded into 3mL printer cartridges and fitted into the BIO X. For the alginate solution, droplets were printed into a calcium chloride (10 mg/mL) crosslinking bath in a ring pattern using 1 ms valve open time, 100 ms drop cycle time, 90 kPa of print pressure, and 10 mm/s print-head translation speed at ambient temperature and allowed to stand for one minute to ensure sufficient crosslinking. The particles were aspirated via pasteur pipette and immersed in phosphate buffered saline. Methacrylated hyaluronic acid (MeHA) solution was printed as water phase droplets into an olive oil (Sigma Aldrich, O1514-500mL) bath using 1 ms valve open time, 100 ms drop cycle time, 50 kPa of print pressure, and 10 mm/s print-head translation speed. The particles were crosslinked using ultraviolet light (OmniCure Series 2000, Excelitas,) at a distance of 15 cm using 100% aperture for 30 seconds. The MeHA spheroids were transferred to a vacuum filtration apparatus, washed 3x with acetone (10mL) to remove oil, and then immersed in phosphate buffered saline.

A. Stiffness Characterization Experiments

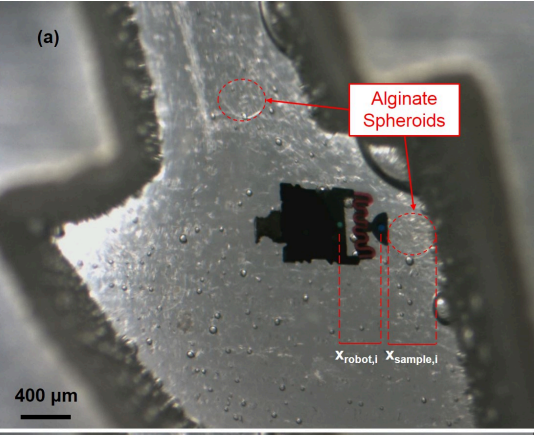
In order to test the stiffness of different types of ECM hydrogel spheroids and other relevant materials, it is important that the spheroid is fixed on one end in such a way that the μ FSMM is able to apply forces on the other end. Figure 4(a) shows the initial position while Fig. 4(b) shows the final position after an alginate spheroid capsule has been pushed against the wall of test fixture. This force application will result in a deformation of both the compliant structure of the microrobot as well as the spheroid itself. Even though the deformation is small, it is still possible to measure nontrivial deformations. The system can be modeled as two springs in series, with stiffnesses k_{robot} and k_{sample} , which undergo deformations, δ_{robot} and δ_{sample} , respectively, when a force, F, is applied. The deformations can be calculated based on the difference in positions, as shown in eq. (1) and (2) below:

$$\delta_{robot} = x_{robot,f} - x_{robot,i} \tag{1}$$

$$\delta_{sample} = x_{sample,f} - x_{sample,i} \tag{2}$$

By pushing and measuring the deflections of the microrobot and the sample, the final stiffness of the sample itself can be computed since the robot's stiffness computed during calibration and is a known value. Thus, Hooke's law can be applied to the model of the system and an expression for k_{sample} can be derived as follows:

$$F = F_{robot} = F_{sample} \tag{3}$$



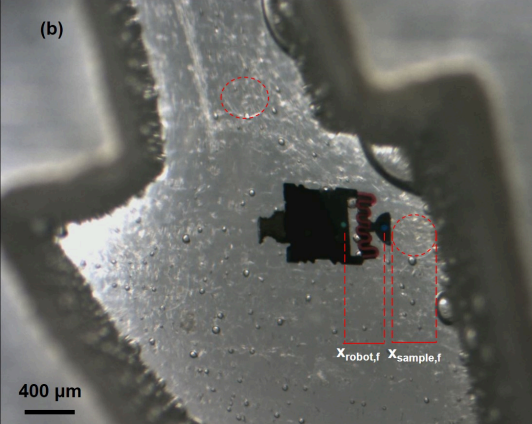


Fig. 4. Experimental setup used for stiffness characterization studies of different materials (a-b): Here, $x_{robot,i}$ and $x_{sample,i}$ refer to the initial distance between two fixed points in the body of the robot and the size of the spheroid, respectively. After the push, these values correspond to $x_{robot,f}$ and $x_{sample,f}$.

$$F_{robot} = k_{robot} \cdot \delta_{robot} \tag{4}$$

$$F_{sample} = k_{sample} \cdot \delta_{sample} \tag{5}$$

$$F = k_{robot} \cdot \delta_{robot} = k_{sample} \cdot \delta_{sample} \tag{6}$$

$$\therefore k_{sample} = \frac{k_{robot} \cdot \delta_{robot}}{\delta_{sample}} \tag{7}$$

Using the μ FSMM, four different types ECM spheroid samples were analyzed to characterize their individual stiffness values. They were hydrogel spheroids, approximately 500 μ m in diameter, made out of alginate and hyaluronic acid, each of them with two different concentrations. Table I shows the robot stiffness and measured sample stiffness in each trial, along with the average stiffness and standard deviation for each material analyzed. As expected, the stiffness of the higher (1%) concentration alginate spheroids is approximately 4x greater than the spheroids with the lower 0.5% alginate concentration sample. The same can be seen for the hyaluronic acid samples, in which the 4% concentration spheroids have an approximately 3.5X higher stiffness than the 2% concentration. In general, since all the samples have similar geometry and sizes, it is expected that different concentration will yield noticeable differences in stiffness, as observed here.

TABLE I

RESULTS FROM STIFFNESS CHARACTERIZATION EXPERIMENTS. NOTE:
UNITS FOR REPORTED STIFFNESS VALUES ARE N/M.

Sample	k_{robot}	k_{sample}	Average k_{sample}	Std. Dev.
Alginate 0.5%	0.43	0.24 0.43 0.22	0.30	0.10
Alginate 1%	0.71	1.43 1.02 1.27	1.24	0.17
Hyaluronic Acid 2%	0.43	0.06 0.07 0.05	0.06	0.01
Hyaluronic Acid 4%	0.43	0.17 0.30 0.17	0.21	0.06

B. Micromanipulation Experiments

In our preliminary micromanipulation tests, it was observed that the required manipulation forces to move the spheroids around the workspace were typically on the order of order of 2 to 4 μ N. There were occasional force spikes observed as well of up to about 15 μ N. These were the result of friction force between the μ FSMM end-effector and the glass substrate and not the actual force being applied to the spheroid. Additionally, the forces applied to the spheroids during the stiffness characterization tests reached around 15μ N, which did not cause any damage to the spheroids. Therefore, since the observed manipulation force values are, on average, much smaller that this, and will not damage the integrity of the spheroids, the real-time monitoring of the forces is not needed for these micromanipulation experiments. Instead, the micromanipulation experiments are focused on the manipulation capabilities of the μ FSMM and the micro-force information is recorded and evaluated offline for verification of safe micromanipulation force levels for biological entities.

Figure 5(a) shows a time lapse of a μ FSMM moving a few spheroids to distances of approximately $100\mu m$ close to each other as a demonstration of the microrobot's micromanipulation capabilities. Considering a cellular context, manipulation of spheroids certain distances from each other is useful for the investigation of paracrine signalling, proliferation, and migration of cells in adjacent spheroids. Additionally, it may prove useful for the in vitro manipulation of drug laden constructs for drug release and therapeutic efficacy on spheroids containing cancerous cells. The force information during the movement of each spheroid is shown in Fig. 5(b). The forces during manipulation are consistent with the ones observed during the preliminary micromanipulation experiments. The force spikes are similarly as a result of the increased friction force experienced between the end-effector and the glass petri dish substrate. Again, the recorded forces are low and the experiment demonstrates that the manipulation does not exceed unsafe forces. Additionally, it can be limited to a set threshold to prevent damage to the spheroids or cells potentially incorporated within the constructs when computing the forces in real-time with closed-loop control, as illustrated in our previous work [23]. Figure 6 demonstrates the μ FSMM ability to accurately position spheroids

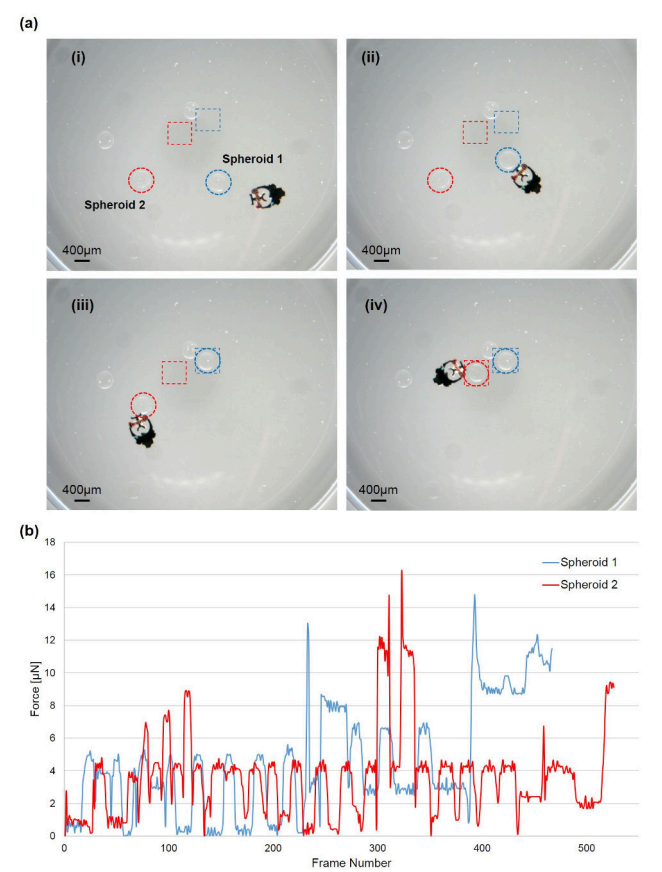


Fig. 5. Micromanipulation experiment: (a) Time lapse of the micromanipulation of two spheroids (red and blue): circles highlight the current position of the spheroids, squares represent their color-coded goal locations. (b) Force information during the micromanipulation of each spheroid.

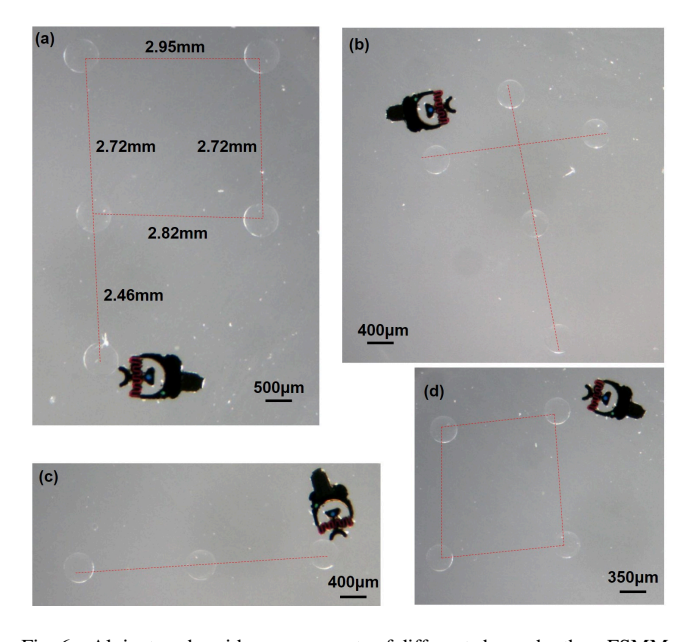


Fig. 6. Alginate spheroids arrangements of different shapes by the μ FSMM: (a) letter P, (b) cross, (c) line, and (d) square.

in different arrangements, useful for the above mentioned applications. A video showcasing the stiffness characterization and example micromanipulation experiments can be found in the supplemental materials.

V. CONCLUSIONS

In this paper, we have presented some of the in vitro biomedical applications of the μ FSMM.The design inherently possesses high flexibility, with different end-effector designs and tunable stiffness depending on the application. Here, the force sensing capabilities of the microrobot were utilized to measure mechanical properties of alginate and hyaluronic acid spheroids with different concentration levels. Furthermore, the μ FSMM successfully managed to micromanipulate these spheroids and place them in desired positions. These experiments showcase the wide range of applications and the impact the microrobot can have in numerous fields of science, including mechanobiology and theranostics. In the future, the μ FSMM can be used in conjunction with a microfluidic device to perform similar types of mechanical testing but with more precision and speed. Furthermore, cellladen spheroids can be manipulated into different placements in order to study their interactions.

ACKNOWLEDGMENTS

The authors acknowledge the facility access at Purdue University's Birck Nanotechnology Center, and technical assistance from Sarah Libring. We would like to thank Dr. Chris Boyer and Cellink for the assistance with the alginate spheroid production.

REFERENCES

- D. R. Frutiger, K. Vollmers, B. E. Kratochvil, and B. J. Nelson, "Small, fast, and under control: wireless resonant magnetic micro-agents," *The International Journal of Robotics Research*, vol. 29, no. 5, pp. 613– 636, 2010.
- [2] S. Kim, S. Lee, J. Lee, B. J. Nelson, L. Zhang, and H. Choi, "Fabrication and manipulation of ciliary microrobots with non-reciprocal magnetic actuation," Sci. Rep., vol. 6, 2016.
- [3] W. Hu, Q. Fan, and A. T. Ohta, "Interactive actuation of multiple optothermocapillary flow-addressed bubble microrobots," *Robot. Biomim.*, vol. 1, no. 14, 2014.
- [4] C. Chen, E. Karshalev, J. Guan, and J. Wang, "Magnesium-based micromotors: Water-powered propulsion, multifunctionality, and biomedical and environmental applications," Small, 2018.
- [5] W. Gao and J. Wang, "Synthetic micro/nanomotors in drug delivery," Nanoscale, vol. 6, no. 18, pp. 10486–10494, 2014.
- [6] M. Sitti, H. Ceylan, W. Hu, J. Giltinan, M. Turan, S. Yim, and E. Diller, "Biomedical Applications of Untethered Mobile Milli / Microrobots," Proceedings of the IEEE, vol. 103, no. 2, pp. 205–224, 2015.
- [7] T. Xu, J. Yu, X. Yan, H. Choi, and L. Zhang, "Magnetic actuation based motion control for microrobotics: An overview," *Micromachines*, vol. 6, no. 9, pp. 1346–1364, 2015.
- [8] P. Hersen and B. Ladoux, "Biophysics: Push it, pull it," *Nature*, vol. 470, no. 7334, pp. 340–341, February 2011.
- [9] Y. Fujii, K. Maru, D.-W. Shu, B. Gu, T. Yamaguchi, R. Lu, T. Jutanggoon, and P. Yupapin, "Material tester with static and dynamic micro forces," *Physics Procedia*, vol. 2, pp. 5–11, 2009. [Online]. Available: www.sciencedirect.comwww.elsevier.com/locate/procedia
- [10] D. E. Jaalouk and J. Lammerding, "Mechanotransduction gone awry," Nature Review, Molecular Cell Biology, vol. 10, pp. 63–73, January 2009
- [11] A. V. Singh and M. Sitti, "Targeted drug delivery and imaging using mobile milli/microrobots: A promising future towards theranostic pharmaceutical design," *Current Pharmaceutical Design*, vol. 22, no. 11, pp. 1418–1428, mar 2016.

- [12] G. Lucarini, V. Iacovacci, P. J. Gouveia, L. Ricotti, and A. Menciassi, "Design of a novel magnetic platform for cell manipulation," *Journal of Micromechanics and Microengineering*, vol. 28, no. 2, 2018.
 [13] J. T. Ko, S. H. Tseng, and M. S. C. Lu, "A CMOS Micromachined
- [13] J. T. Ko, S. H. Tseng, and M. S. C. Lu, "A CMOS Micromachined Capacitive Tactile Sensor with High-Frequency Output," *Journal of Microelectromechanical Systems*, vol. 15, pp. 1708–1714, 2006.
- [14] F. Beyeler, S. Muntwyler, Z. Nagy, S. Muntwyler, F. Beyeler, and B. J. Nelson, "Three-axis micro-force sensor with sub-micro-Newton measurement uncertainty and tunable force range," *Journal of Mi*cromechanics and Microengineering, vol. 20, p. 8, 2010.
- [15] S. Guo, X. Zhu, D. Jańczewski, S. Siew Chen Lee, T. He, S. Lay Ming Teo, and G. Julius Vancso, "Measuring protein isoelectric points by AFM-based force spectroscopy using trace amounts of sample," *Nature Nanotechnology* I, vol. 11, 2016. [Online]. Available: www.nature.com/naturenanotechnology
- [16] Y. M. Efremov, W.-H. Wang, S. D. Hardy, R. L. Geahlen, and A. Raman, "Measuring nanoscale viscoelastic parameters of cells directly from AFM force-displacement curves," vol. 7, no. 1541, 2017. [Online]. Available: www.nature.com/scientificreports/
- [17] G. Wang and Q. Xu, "Design and precision position/force control of a piezo-driven microinjection system," *IEEE/ASME Transactions on Mechatronics*, vol. 22, no. 4, pp. 1744–1754, 2017.
- [18] R. Schulze, T. Gessner, M. Heinrich, M. Schueller, R. Forke, D. Billep, M. Sborikas, and M. Wegener, "Integration of Piezoelectric Polymer Transducers into Microsystems for Sensing Applications," *Proceedings* of ISAF/ECAPD/PFM, pp. 1–4, 2012.
- [19] J. Wei, M. Porta, M. Tichem, U. Staufer, and P. M. Sarro, "Integrated piezoresistive force and position detection sensors for micro-handling applications," *Journal of Microelectromechanical Systems*, vol. 22, no. 6, pp. 1310–1326, Dec. 2013.
- [20] S. D. Bhargav, N. Jorapur, and G. Ananthasuresh, "Micro-scale composite compliant mechanisms for evaluating the bulk stiffness of mcf-7 cells," *Mechanism and Machine Theory*, vol. 91, pp. 258 – 268, 2015.
- [21] D. J. Cappelleri, G. Piazza, and V. Kumar, "A two dimensional vision-based force sensor for microrobotic applications," *Sensors & Actuators: A. Physical*, vol. 171, pp. 340–351, 2011.
- [22] M. Guix, J. Wang, Z. An, G. Adam, and D. J. Cappelleri, "Real-Time Force-Feedback Micromanipulation Using Mobile Microrobots With Colored Fiducials," *IEEE Robotics and Automation Letters*, 2018.
- [23] W. Jing, S. Chowdhury, M. Guix, J. Wang, Z. An, B. V. Johnson, and D. J. Cappelleri, "A Microforce-Sensing Mobile Microrobot for Automated Micromanipulation Tasks," *IEEE Transactions on Automation Science and Engineering*, pp. 1–13, 2018.
- [24] M. Sun, G. Chi, P. Li, S. Lv, J. Xu, Z. Xu, Y. Xia, Y. Tan, J. Xu, L. Li, and Y. Li, "Effects of matrix stiffness on the morphology, adhesion, proliferation and osteogenic differentiation of mesenchymal stem cells," *Int J Med Sci*, vol. 15, pp. 257–268, 2018. [Online]. Available: http://www.medsci.org/v15p0257.htm
- [25] Z. Razinia, P. Castagnino, T. Xu, A. Vázquez-Salgado, E. Puré, and R. K. Assoian, "Stiffness-dependent motility and proliferation uncoupled by deletion of cd44," in *Scientific Reports*, 2017.
- [26] O. Chaudhuri, S. Koshy, C. Branco da Cunha, J.-w. Shin, C. Verbeke, K. Allison, and D. Mooney, "Extracellular matrix stiffness and composition jointly regulate the induction of malignant phenotypes in mammary epithelium," *Nature Mater*, vol. 13, p. 970–978, 2014.
- [27] S. Dupont, L. Morsut, M. Aragona, E. Enzo, S. Giulitti, M. Cordenonsi, F. Zanconato, J. Le Digabel, M. Forcato, S. Biccato, N. Elvassore, and S. Piccolo, "Role of YAP/TAZ in mechanotransduction," *Nature*, vol. 474, pp. 179–183, 2011.
- [28] Y. Hirose, M. Kaneko, T. Kawahara, Y. Yamanishi, and F. Arai, "High speed cell stiffness evaluation toward 100% reliability," in SENSORS, 2011 IEEE, Oct 2011, pp. 962–965.
- [29] S. Sakuma, K. Nakahara, and F. Arai, "Continuous mechanical indexing of single-cell spheroids using a robot-integrated microfluidic chip," *IEEE Robotics and Automation Letters*, vol. 4, no. 3, pp. 2973–2980, July 2019.
- [30] A. Blumlein, N. William, and J. McManus, "The mechanical properties of individual cell spheroids," Sci Rep, vol. 7, p. 7346, 2017.
- [31] D. Jaiswal, N. Cowley, Z. Bian, G. Zheng, K. P. Claffey, and K. Hoshino, "Stiffness analysis of 3d spheroids using microtweezers," *PLOS ONE*, vol. 12, no. 11, pp. 1–21, 11 2017.
- [32] K. A. Smeds and M. W. Grinstaff, "Photocrosslinkable polysaccharides for in situ hydrogel formation," *Journal of Biomedical Materials Research*, vol. 54, no. 1, pp. 115–121, 2001.